Journal of Materials Chemistry A

Accepted Manuscript

ROYAL SOCIETY OF CHEMISTRY

www.rsc.org/materialsA

Journal of Materials Chemistry A

ARTICLE

Electrospun Cobalt Embedded in Porous Nitrogen Doped Carbon Nanofibers as an Efficient Catalyst for Water Splitting

Received 00th January 20xx,
Accepted 00th January 20xx

DOI: 10.1039/x0xx00000x

www.rsc.org/

Yufei Zhao[a,b], Jinqiang Zhang[b], Kefei Li[b], Zhimin Ao[b], Chengyin Wang[c], Hao Liu[b,*], Kening Sun[a,*], Guoxiu Wang[b,*]

The major challenge in water splitting is to develop low cost electrocatalysts as alternatives for simultaneously generating oxygen and hydrogen. Herein, we report the successful synthesis of cobalt nanoparticles embedded in porous nitrogen doped carbon nanofibers (Co-PNCNFs) by a facile and scalable electrospinning technology. The electrospun Co-PNCNFs composite exhibits a low onset potential of 1.45 V (*vs*. RHE) along with high current density (overpotential of 285 mV for 10 mA cm^{-2}) towards oxygen evolution reaction (OER). The exceptional performance could be ascribed to the bi-functionalized CNFs with nitrogen doping and cobalt encapsulation. Moreover, the porous structure and synergistic effect further provide high effective surface area and facilitate a fast electron transfer pathway for the OER process. Interestingly, the Co-PNCNFs composite also displays the capability for hydrogen evolution reaction (HER) in alkaline solution. A water electrolyzer cell fabricated by applying Co-PNCNFs as both anode and cathode electrocatalysts in alkaline solution can achieve a high current density of 10 mA cm^{-2} at a voltage of 1.66 V.

Introduction

With increasing demand for renewable energy, there are intense efforts to develop various types of energy storage and conversion systems.[1] Electrocatalytic oxygen evolution reaction (OER) and hydrogen evolution reaction (HER) are the key steps in many renewable energy processes, including fuel cells, water splitting and rechargeable metal-air batteries.[2-5] Currently, typical catalysts used for OER and HER in electrolysis cells are still precious metal-based materials (Pt, RuO_2, IrO_2) because of their outstanding catalytic activities.[6,7] Nevertheless, their mass productions have been limited by the high cost and low-abundance. Over the last few decades, considerable efforts have shifted to the development of non-precious-element materials as catalysts for water splitting due to their abundance and promising catalytic properties.

Recently, a variety of cost-effective materials have been tested for catalyzing the electrochemical hydrogen evolution, including transition-metal chalcogenides,[8,9] carbides,[10,11] and complexes.[12] Furthermore, OER with more sluggish kinetics also requires efficient catalysts (cobalt oxides (CoO, Co_3O_4), substituted cobaltites $M_xCo_yO_4$ (M = Ni, Fe)) to reduce the energy barrier and further accelerate the overall water splitting process.[13-16] Nitrogen/transition metal (Co, Ni, Fe) functionalized carbon materials have been developed as the most promising candidates for HER, OER and even oxygen reduction reaction (ORR) due to their high catalytic performances.[17,18] The morphology, structure and electronic conductivity are the key factors influencing their electrocatalytic efficiency.[19] However, the corrosion property and poor stability of the transition metals may result in poor performances during the test. Recently, in order to further enhance the catalytic activity and stability, there are a few works reported based on the encapsulated structure, such as Co, Fe or FeCo, NiCo alloy nanoparticles embedded in nitrogen–doped carbon materials (carbon nanotubes or graphene), and these catalysts delivered high performance towards OER, HER or ORR.[20-23] The confinement of these composites not only provides an easy way to restrict the size of the encapsulated particles down to the nanometer scale, but also creates unique structural features with well-developed interactions between the encapsulated metal particles and the carbon materials. However, it is still a great challenge to create an effective way to disperse metal particles uniformly encapsulated by the carbon materials. Thus, developing a simple and scalable technique (e.g. electrospinning) to produce high performance electrocatalysts with the unique encapsulated structure is highly desirable, especially as catalysts towards overall water splitting.

Carbon nanofibers (CNFs), a popular one dimensional carbon material, have already garnered extensive interests due to their attractive properties of high electronic conductivity and good electrochemical stability, which can be synthesized by a

[a] *Beijing Key Laboratory for Chemical Power Source and Green Catalysis, School of Chemical Engineering and Environment, Beijing Institute of Technology, Beijing, 100081, China. E-mail: bitkeningsun@163.com*
[b] *Center for Clean Energy Technology, School of Mathematical and Physical Science, Faculty of Science, University of Technology Sydney, NSW 2007, Australia Email: Hao.Liu@uts.edu.au; Guoxiu.Wang@uts.edu.au,.*
[c] *College of Chemistry and Chemical Engineering, Jiangsu Key Laboratory of Environmental Engineering and Monitoring, Yangzhou University, 180 Si-Wang-Ting Road, Yangzhou, 225002, China.*
Electronic Supplementary Information (ESI) available: [details of any supplementary information available should be included here]. See DOI: 10.1039/x0xx00000x

facile electrospinning technique.[24-28] To date, only a few studies have been investigated by using electrospun materials as the catalysts.[29,30] Generally, CNFs merely work as matrix for providing large specific surface area and enhancing conductivity for the catalysts. The contribution for the catalytic performance directly from carbon is usually ignored. As above mentioned, functionalized carbon (CNTs or graphene) with transition metal or nitrogen element could efficiently convert the inert carbon into active sites as electrocatalysts.[31,32] Therefore, it is significant to design novel functionalized CNF-based catalysts by electrospinning technique for water splitting.

Herein, we developed a facile, scalable method to synthesize cobalt nanoparticles embedded in porous nitrogen doped CNFs (Co-PNCNFs) by electrospinning technique. The Co-PNCNFs composite displays a well-defined 3D networks associated with encapsulated and porous structure. The unique encapsulated structure could efficiently avoid the metal nanoparticles directly contact with the harsh environmental, protecting the metal nanoparticles from corrosion and aggregation during the catalytic process. The porous structure could provide more active sites for oxygen evolution and facilitate fast and versatile transport pathways for the electrolyte diffusion. Benefiting from its high exposed effective surface area, improved electronic conductivity, intimate interaction and synergetic effect, Co-PNCNFs can serve as active electrocatalyst for both OER and HER with an outstanding performance and excellent stability.

Experimental

Synthesis

Synthesis of Co-PNCNFs: Co-PNCNFs were prepared using an electrospinning method with a subsequent heat treatment. All the chemicals were of analytical grade and were used without further purification. 320 mg of cobalt nitrate ($Co(NO_3)_2 \bullet 6H_2O$, >98%, Sigma-Aldrich) and 600 mg of polyacrylonitrile (PAN, M_w = 150,000 g mol^{-1}, Sigma-Aldrich) were dissolved in 6 ml N,N-dimethylformamide (DMF, 99.8%, Chem-supply). The above solution was left at 50 ˚C under vigorous stirring overnight and then transferred to a 10 ml plastic syringe with a 20-gauge blunt tip needle. For the electrospinning, a high voltage of 18 kV and flow rate of 14.8 µl min^{-1} were applied, with a distance of 15 cm between the needle and rotating grounded collector. The as-collected electrospun fibers first underwent heat treatment at 450 ˚C for 2 h in an H_2 (H_2 : Ar = 5 : 95 vol%) atmosphere and then 800 ˚C for 6 h in Ar atmosphere to obtain the composite (Co-NCNFs). The heating rate was kept at 1 ˚C min^{-1}. Cobalt nanoparticles loaded on the surface of CNFs were removed by washing in 0.5 M H_2SO_4 solution for 24 h to achieve the porous structure composite (Co-PNCNFs).

Synthesis of NCNFs: The preparation process of the pure N-doped CNFs (NCNFs) was the same as the method used for Co-PNCNFs, but without the addition of cobalt nitrate in the electrospinning solution.

Synthesis of the comparison materials: Nickel or iron embedded in porous nitrogen doped CNFs (Ni-PNCNFs, Fe-PNCNFs) were prepared by replacing cobalt nitrate with nickel nitrate or iron nitrate. Cobalt embedded in carbon nanofibers (Co-PCNFs) were fabricated by using polyvinylpyrrolidone (PVP M_w = 360000 g mol^{-1}) to replace PAN.

Characterization

The morphology and particle size of the samples were acquired with field emission scanning electron microscopy (FESEM, Zeiss Supra 55VP), element mapping and electron energy dispersive spectroscopy (Zeiss Evo SEM), and transmission electron microscopy (TEM, Model JEM-2011, JEOL). X-ray diffraction (XRD) of the samples was characterized by employing a scanning step of 0.02˚ per second in the 2 θ range from 10 to 80˚ (Siemens D5000 using Cu Kα radiation). Raman spectra were obtained on an inVia Renishaw Raman spectrometer system (HR Micro Raman spectrometer, Horiba JOBIN YVON US/ HR800 UV) using a 632.8 nm wavelength laser. X-ray photoelectron spectroscopy (XPS) was collected on an ESCALAB250Xi (Thermo Scientific, UK) equipped with mono-chromated Al K alpha (energy 1486.68 eV). Brunauer–Emmett–Teller (BET) surface area of the obtained materials was achieved by using experimental points at a relative pressure of P/P_0 = 0.05–0.25. Thermogravimetric analysis (TGA) was performed by simultaneous TG-DTA (SDT 2960) at a heating rate of 5 ˚C min^{-1} from room temperature to 800 ˚C in air atmosphere.

Electrochemical Measurements

The electrocatalytic experiments were carried out on an electrochemical workstation (CHI 660E)**.** Data were collected in a standard three-electrode glass cell, with platinum wire and Ag/AgCl (saturated KCl) working as the counter and reference electrodes ($E_{RHE} = E_{Ag/AgCl} + 0.059 \times pH + 0.1971$), respectively. OER and HER performance were tested by using materials on GC as working electrodes. The working electrode was fabricated as follows: the catalyst slurry was prepared by mixing 4 mg of catalyst, 80 μl of Nafion (5 wt %) and 1 ml solvent (1:1 v/v water/isopropanol) and then sonicated for 30 min to form a dispersion. 10 μl of the dispersion was dropped onto the glassy carbon (GC) electrode with the mass loading of 0.56 mg cm^{-2} (diameter of 3 mm), followed by drying at room temperature. Water electrolyzer tests were performed by using Co-PNCNFs on the Ni foam for water splitting. To prepare Co-PNCNFs on the Ni foam, 16 mg catalyst were dispersed in 2 ml solvent (1:1 v/v water/isopropanol, 200 μl of Nafion). After sonication, 1 ml of the suspension was dropped onto 1 × 1 cm Ni foam (8 mg cm^{-2}) and then dried in the vacuum oven at 80 ˚C. OER or HER activities of the catalysts were evaluated by linear sweep voltammetry (LSV) in 1 M KOH solution at a scan rate of 5 mV s^{-1}. The polarization curves were all corrected for the *i*R contribution within the cell. The electrochemical impedance spectra were obtained by applying an amplitude of 5 mV within a frequency ranges from 10^6 to 0.01 Hz under open circuit. The effective surface area of Co-PNCNFs and NCNFs were evaluated by cyclic voltammetry (CV), conducted in a potential range in which no apparent Faradaic processes occur at different scan rates (10 to 100 mV s^{-1}). The

cycling performance of Co-PNCNFs based electrode was operated by repeating LSV running for 5000 cycles with the potential range from 1.20 to 1.70 V *vs*. RHE and the current–time plots were performed with the applied potentials at 1.52 or 1.54 V (*vs*. RHE).

The rotating ring-disk electrode (RRDE) voltammograms were carried out based on an RRDE configuration (Pine Research Instrumentation, USA) with a GC disk and Pt ring electrode. The as-prepared Co-PNCNFs catalyst was coated onto the disk electrode by using the above mentioned method. A rotating speed of the RRDE was held at 1600 rpm for the test. To ensure the oxidation current originated from oxygen evolution, the ring potential was held constantly at 0.45 V *vs*. RHE (disk current fixed at 250 μA) to reduce the formed O_2 from the catalyst on the disk in N_2-saturated 1 M KOH solution. A continuous OER (disk electrode) → ORR (ring electrode) process occurred on the RRDE. The Faradaic efficiency was calculated as follows: $\varepsilon = I_r/(I_d N)$, where I_d is the disk current, I_r is the ring current, and N represents the current collection efficiency of the RRDE (N = 0.2).[33-35] On the other hand, to detect the hydrogen peroxide (HO_2^-) formation, the ring potential was held constantly at 1.50 V *vs*. RHE for oxidizing HO_2^- intermediate in O_2-saturated 1 M KOH (the disk potential was held constantly at 1.55 V *vs*. RHE).

Results and Discussion

Fig. 1 illustrates the preparation of Co-PNCNFs nanofibers by electrospinning. The electrospun nanofibers were collected on the substrate, followed by the reduction in H_2/Ar and carbonization in Ar atmosphere. The nitrogen-rich PAN provides a good strategy to form N-doped carbon materials, which is an efficient approach to improve the catalytic activity of carbon-based materials. The final material of Co-PNCNFs was obtained by acid treatment to remove the cobalt nanoparticles on the surface of CNFs. The yield of the product (Co-PNCNFs) is around 70%, based on the theoretic transformation of raw materials.

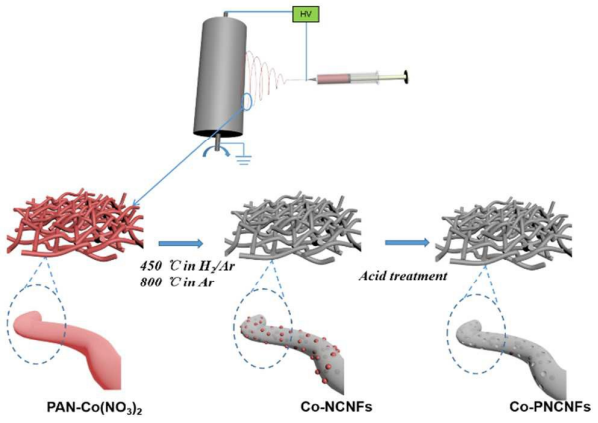

Fig. 1 Schematic illustration for the preparation of Co-PNCNFs nanofibers by electrospinning.

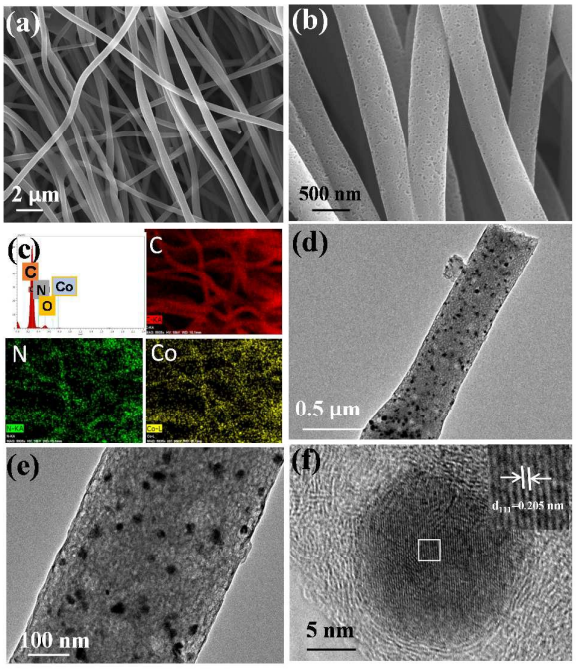

Fig. 2 Electron microscopy characterization of Co-PNCNFs. (a) low magnification and (b) high magnification SEM images of Co-PNCNFs. (c) EDS analysis of Co-PNCNFs, showing homogenous distribution of C, N, Co elements in fibrous structure. (d) TEM image of a single fibrous Co-PNCNF. (e) Enlarged TEM image of a single Co-PNCNF, demonstrating the structure of dispersed nanoparticles embedded in porous carbon fiber. (f) HRTEM image of a Co nanoparticle wrapped in carbon. The inset is the enlarged area as denoted in the white box, displaying an interplanar spacing of 0.205 nm.

Fig. 2a and b show the SEM images of Co-PNCNFs. Co-PNCNFs display a well-organized 1-D cylindrical morphology, forming continuous carbon fiber networks. The high magnification SEM image of Co-PNCNFs (Fig. 2b) reveals that the average diameter of the electrospun nanofibers was around 400-500 nm, and no cobalt nanoparticles could be observed on the surface of CNFs. More importantly, the high magnification image indicates that the surface of Co-PNCNFs is rougher and more porous compared with the pure NCNFs (Fig. S1), owing to the removal of cobalt particles with acid treatment. Energy dispersive spectroscopy (EDS) and element mapping confirm that Co-PNCNFs are composed of C, N, Co, O elements, with homogenous distribution (Fig. 2c and Fig. S3). TEM characterization in Fig. 2d further verifies that the particles on the surface of CNFs are all removed and only small cobalt nanoparticles (10-20 nm) encapsulated in CNFs can be observed. These carbon-encased cobalt nanoparticles are not exposed, as they remain embedded in CNFs even after being treated with acidic solution. In Fig. 2e, the high magnification TEM image clearly shows the porous structure formed on the surface of Co-PNCNFs. Fig. 2f displays a single cobalt nanoparticle with size of 15 nm embedded in carbon fiber. The formation of a few layers onion–like graphitic carbon wrapped

around the encapsulated Co nanoparticle can be ascribed to the catalytic effect of Co nano-catalyst during the carbonization process. The inset of Fig. 2f represents the enlarged area as denoted in white box, showing a d-spacing of 0.205 nm for the nanoparticles, which can be indexed to the (111) interplanar plane of cobalt.

Fig. 3a shows the XRD patterns of the final materials of NCNFs and Co-PNCNFs. The diffraction peaks around 25.2˚ for NCNFs and Co-PNCNFs are attributed to the (002) crystallographic plane of graphite, indicating that the graphitic structure has been obtained after carbonization (corresponding to the HRTEM result). The presence of metallic cobalt in Co-PNCNFs is manifested by the two peaks around 43.8˚and 51.9˚, which can be indexed to the (111) and (200) crystal planes of the cobalt (PDF No. 15-0806), suggesting the successful reduction of cobalt ions to a metallic state during carbonization. And the d-spacing of cobalt (111) calculated from XRD peak by Bragg equation (2d sin θ = nλ (n=1, λ=0.154056 nm)) is 0.2065 nm, which is quite close to the HR-TEM observation (d=0.205 nm). The low diffraction peaks of Co can be ascribed to the small amount of metallic cobalt in the composite (11.4 wt %, TGA, Fig. S5). Fig. 3b represents the typical Raman spectra of NCNFs and Co-PNCNFs that display two typical peaks, corresponding to the defect induced D-band and graphitic G-band, respectively.[25,36] The intensity ratio of D/G (I_D/I_G) value for Co-PNCNFs hybrid (1.17) is higher than that of pure NCNFs (1.08). The increased I_D/I_G indicates more defects in the carbon lattice of Co-PNCNFs, which may be as a result of the removal of cobalt nanoparticles (porous structure) and the defects in the graphitic structures. From the XPS survey spectrum of Co-PNCNFs in Fig. 3c, only C, N and O elements can be clearly observed, and there is no distinguishable signal for Co, because of its low content and encapsulation in carbon matrix (XPS spectrum of NCNFs is shown in Fig. S6a). The high resolution XPS spectrum in Fig. 3d shows the characteristic peak located at 777.6 and 793.3 eV, attributing to the property of Co 2p. The high resolution N 1s spectrum (Fig. 3e) could be deconvoluted into two peaks (same results for NCNFs, Fig. S6b), corresponding to the pyridinic (398.4 eV) and pyrrolic N (401.2 eV), both of which have been proven to have efficient catalytic activity towards OER and HER.[22,37] Based on the XPS result, the percentage of Nitrogen in Co-PNCNFs is ~5.44 wt%. The BET surface area of Co-PNCNFs is 356.6 m^2 g^{-1} (Fig. 3f), which is much higher than that of NCNFs (8.7 m^2 g^{-1}, Fig. S7). This should be attributed to the unique porous structure of Co-PNCNFs (Pore size distribution of Co-PNCNFs is shown in the inset of Fig. 3f, displaying the presence of mesopores at 7 nm). The Co-PNCNFs with larger surface area are expected to provide more active sites for the water splitting reaction.

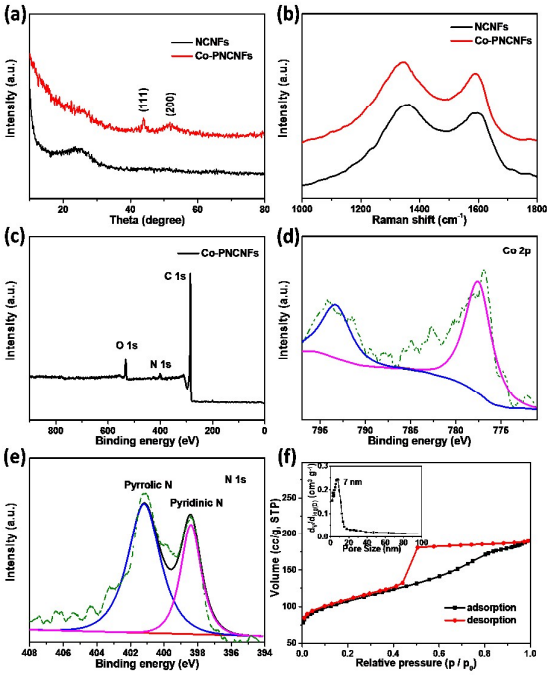

Fig. 3 (a) XRD patterns of NCNFs and Co-PNCNFs. (b) Raman spectra of NCNFs and Co-PNCNFs. (c) XPS spectrum of Co-PNCNFs composite. High resolution XPS spectra of (d) Co 2p and (e) N 1s. (f) Nitrogen sorption isotherm of Co-PNCNFs, inset shows the pore size distribution of Co-PNCNFs.

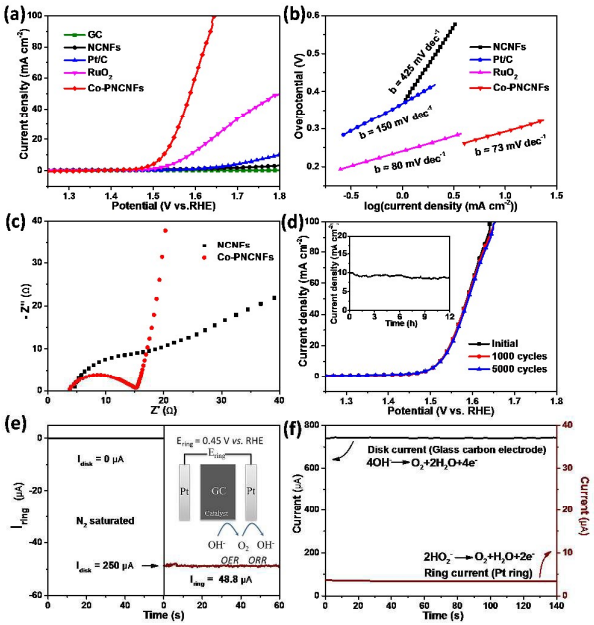

Fig. 4 Electrochemical performance of the catalysts towards OER in 1 M KOH solution: (a) Polarization curves for Co-PNCNFs, NCNFs, RuO_2, Pt/C and pure GC. (b) The corresponding Tafel plots of catalysts. (c) Nyquist plots of Co-PNCNFs and NCNFs modified electrodes. (d) Stability test of Co-PNCNFs through potential cycling, displaying polarization curves of initial one, after 1000 and 5000 potential cycles. Inset shows the chronoamperometric stability test over 12 h. (e) The ring current of Co-PNCNFs on a RRDE (1600 rpm) in a N_2-saturated 1 M KOH solution (ring potential: 0.45 V *vs.* RHE). (f) Disk and ring current of Co-PNCNFs on a RRDE (1600 rpm) with a disk potential of 1.55 V (*vs.* RHE) and ring potential of 1.50 V (*vs.* RHE) in 1 M KOH solution.

The electrocatalytic activities of the catalysts (Co-PNCNFs, NCNFs, RuO_2, Pt/C) were investigated for OER in 1 M KOH solution by LSV. As shown in Fig. 4a, Co-PNCNFs exhibit the highest catalytic activity with a low onset potential of 1.45 V (*vs*. RHE), above which the anodic current rises rapidly. The current density of 10 mA cm^{-2} could be achieved at a low overpotential of 285 mV for Co-PNCNFs. This catalytic activity of Co-PNCNFs is superior to the behaviour of non-noble electrocatalysts at the same condition for OER, such as the exfoliated NiCo layered double hydroxide nanosheets, (367 mV for 10 mA cm^{-2}), Ni–Co double hydroxides nanocages (350 mV for 10 mA cm^{-2}) and ($Co_yFe_{10-y}O_x$/NPC) nanosheets (328 mV for 10 mA cm^{-2}).[38-40] Moreover, the catalytic activities of the deposited materials (including the commercial standard catalysts) were compared by recording their current densities at an overpotential of 400 mV. Co-PNCNFs exhibits the highest catalytic current density of 86 mA cm^{-2} (20 mA cm^{-2} for RuO_2, 2.5 mA cm^{-2} for Pt/C, 1.3 mA cm^{-2} for NCNFs) and no OER catalytic activity for the bare GC electrode. Tafel slopes are derived from the polarization curves in Fig. 4a to gain insight into the OER process. The corresponding Tafel slope of Co-PNCNFs based electrode, 73 mV dec^{-1}, is much lower than that of pure NCNFs (425 mV dec^{-1}), indicating that the introduction of cobalt can deliver a much more favourable reaction kinetics and provide a remarkably increased OER rate with the increase of overpotentials (drive a large catalytic current density at low overpotential). Co-PNCNFs deliver outstanding electrocatalytic performance as an efficient OER catalyst, including low overpotential, high catalytic current density and small Tafel slope. This enhancement can be ascribed to the unique porous 3D network architecture, and bi-functionalization with cobalt encapsulation and nitrogen doping.

To probe the effect of the structure and component of the catalysts on the OER process, effective surface area and electrochemical impedance spectra (EIS) were measured for Co-PNCNFs and NCNFs catalysts. Co-PNCNFs can provide a larger effective surface area, which can be evaluated approximately by using electrochemical double-layer capacitance (C_{dl}).[41,42] Co-PNCNFs exhibit an 18.7-times C_{dl} (26.2 mF cm^{-2}) than that of pure NCNFs (1.4 mF cm^{-2}) (Fig. S8). Generally, the higher effective surface area is contributed to the higher electrocatalytic activity of the Co-PNCNFs composite. Fig. 4c shows the EIS results, in which both Co-PNCNFs and NCNFs display a semicircle in the high frequency region and a straight-line in low frequency region, indicating the similar mass transport properties and reaction kinetics for OER process. It should be noted that Co-PNCNFs exhibit much lower impedance than that of NCNFs.

Besides high catalytic activities, good stability towards water splitting is also a critical aspect for an energy conversion system. To assess the stability of the catalyst, long-term potential cycling of Co-PNCNFs modified GC electrode was carried out in an alkaline solution by recording continuous LSVs for 5000 cycles. As shown in Fig. 4d, the polarization curves of Co-PNCNFs towards OER for the initial, 1000th and even 5000th cycles are identical, with negligible decrease of the current density. Furthermore, the practical operation of the catalyst is usually examined by electrolysis at the fixed potentials. The current–time plots of the Co-PNCNFs based electrode with the applied potentials at 1.52 V and 1.54 V (*vs*. RHE) are presented in the inset of Fig. 4d and S9a. The stable current density for 12 h and 60 h continuous operation suggests that the Co-PNCNFs electrode has a good durability for water splitting. The *ex-situ* SEM image (Fig. S9b) implies the excellent stability of fibrous Co-PNCNFs towards long term testing. Such stable characteristic should originate from the N-doped carbon nanofiber matrix and the protected cobalt nanoparticles embedded in CNFs. The durability of the Co-PNCNFs catalyst demonstrates the potential for practical applications.

To ensure that the observed oxidation current in Fig. 4a originates from oxygen evolution rather than other side reactions and to calculate the Faradaic efficiency, RRDE apparatus was applied in N_2-saturated 1 M KOH solution, rendering a continuous OER (disk electrode)-ORR (ring electrode) process.[33-35] With the disk current fixed at 250 μA, O_2 molecules generated from the Co-PNCNFs catalyst, and the formed O_2 molecules were further reduced by sweeping across the surrounding Pt ring electrode with an ORR potential of 0.45 V *vs*. RHE. As shown in Fig. 4e, a ring current of approximately 48.8 μA can be detected (RRDE collection efficiency = 0.2), corresponding to a Faradaic efficiency of 97.6% (see calculation details in the Experimental part). Furthermore, we have analyzed the content of the HO_2^- intermediates formed at the surface of Co-PNCNFs catalyst during the OER process by employing Pt ring electrode potential at 1.50 V *vs*. RHE (disk potential was fixed at 1.55 V *vs*. RHE). Fig. 4f shows a relatively low ring current value (~ 3.3 μA) compared to that of disk current (~ 740 μA), suggesting that the formation of by-product (HO_2^-) is negligible and the OER reaction occurs via a desirable four-electron pathway for water oxidation, *i.e.* $4OH^- \rightarrow O_2 + 2H_2O + 4e^-$.

The above mentioned results demonstrate that the Co-PNCNFs catalyst exhibits excellent electrocatalytic performance towards OER. Based on the aforementioned measurements and coupled with recent studies on nitrogen doped carbon materials or Co-based electrocatalysts, the following synergistic catalytic factors are proposed to elaborate the enhanced OER activity of the Co-PNCNFs catalyst. First, the unique one dimensional structure, as well as its porous architecture with high specific surface area, provides high catalyst/electrolyte interfaces for oxygen evolution. Therefore, a large amount of active sites are generated, leading to the enhanced catalytic activities. Second, the cobalt/CNF core-shell structure benefits for the OER process in many aspects. Even though the metals (Co, Ni, Fe; the electrochemical performance of Ni-PNCNFs, Fe-PNCNFs are presented in Fig. S11a, 12) are not in direct contact with the electrolyte, they can influence the property of protective carbon towards catalytic processes. It is proposed that the catalytic activity might come from the structural and electronic interaction between the encapsulated metal and the protective carbon, and their intimate and direct contact further induce a high electronic conductivity, which promotes

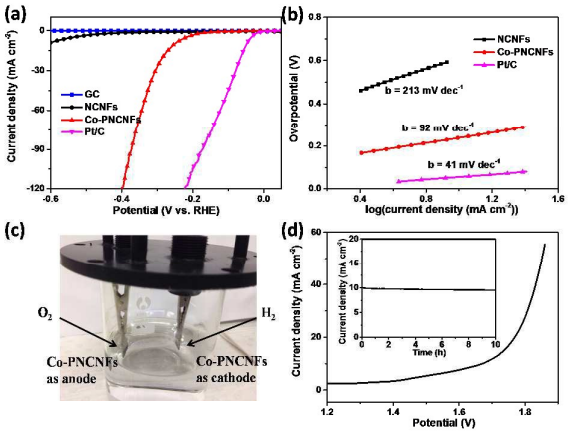

Fig. 5 Electrochemical performance of the catalysts towards HER in 1 M KOH solution: (a) polarization curves for Co-PNCNFs, NCNFs, Pt/C and bare GC. (b) The corresponding Tafel plots. (c) Optical photograph of Co-PNCNFs based electrolyzer. (d) LSV of water electrolysis using Co-PNCNFs as both OER and HER catalysts. The inset shows the stability test at the potential of 1.66 V over 10 h.

the OER activity.[43-46] Furthermore, the Co-PNCNFs catalyst is structurally stable in electrolyte because the metal nanoparticles are efficiently protected by encapsulated structure, so that outstanding long term performance can be achieved. Third, the positively charged nitrogen dopant in the carbon lattice could not only improve the interaction with reactant, but also induce asymmetrical charge distributions on the adjacent carbon atoms (facilitate a fast electron transfer for OER), resulting in the acceleration of the dynamics of oxygen evolution (the electrochemical performance of Co-PCNFs without nitrogen doping is presented in Fig. S11b).[31,47-49] Lastly, the encapsulated metallic cobalt nanoparticles and the nitrogen dopant synergistically affect the microstructure of the composite, not only by converting the inert carbon atoms into active sites, but also significantly improving the charge transport of electrodes, which efficiently reduces the reaction barrier and enhances the catalytic performance.

Co-PNCNFs have also shown efficient catalytic activity towards hydrogen evolution. The electrocatalytic activity of the Co-PNCNFs catalyst for HER was examined in 1 M KOH solution. According to the polarization curves (Fig. 5a), it is evident that Co-PNCNFs exhibit acceptable catalytic activity towards HER. The catalyst achieved 10 mA cm^{-2} at an overpotential of 249 mV, which is better than that of previously reported Co-NRCNTs (370 mV for 10 mA cm^{-2}) at the same condition.[21] Moreover, Co-PNCNFs displayed a smaller Tafel slope of 92 mV dec^{-1} (Fig. 5b) than that of the pure NCNFs (213 mV dec^{-1}). These findings confirm the good electrocatalytic activity of Co-PNCNFs towards HER in alkaline solution. The catalytic stability was further evaluated by running continuous LSVs for 1000 cycles. Almost no change was observed from the polarization curves (Fig. S13).

The good catalytic activity and durability for both OER and HER suggest that the Co-PNCNFs composite is a highly efficient catalyst for the overall water splitting reaction in alkaline media. To test the feasibility, we fabricated the water splitting electrolyzer by applying Co-PNCNFs both as the anode and cathode in 1 M KOH solution, respectively (Fig. 5c, the OER and HER performance of Co-PNCNFs deposited on Nickel foam are shown in Fig. S14). At room temperature, the water electrolyzer reaches a current density of 10 mA cm^{-2} at 1.66 V, which is competitive to recently published references (Fig. 5d, the comparison data are listed in Table S1). The durability of the electrolyzer was tested at 1.66 V in 1 M KOH solution. As shown in the inset of Fig. 5d, the cell exhibits excellent stability for the overall water splitting. The high performance and long durability of the Co-PNCNFs catalyst in the alkaline electrolyzer provides a new strategy for developing non-precious efficient catalyst for the overall water splitting.

Conclusions

In summary, the Co-PNCNFs composite with small cobalt nanoparticles embedded in N-doped porous carbon nanofibers was prepared by electrospinning and evaluated as a catalyst for OER and HER in alkaline solution. The excellent OER performance (high catalytic activity and good stability) was obtained, owing to the unique encapsulated and porous architecture. The nitrogen and cobalt bi-functionalization CNFs generates active sites, which have a significant synergic effect on enhancing the catalytic activity. Moreover, the Co-PNCNFs composite also demonstrates a catalytic effect on the HER process in alkaline media. The excellent performance of the Co-PNCNFs composite towards both OER and HER makes it as an efficient catalyst for the overall water splitting. The alkaline electrolyzer achieves 10 mA cm^{-2} at a voltage of 1.66 V with a long durability. We believe that such transition metal embedded in low dimensional carbon matrix materials (e.g. Co-PNCNFs) can be practically applied as high-performance catalysts for overall water splitting.

Acknowledgements

This project is financially supported by the Australian Research Council (ARC) through the ARC Discovery project (DP1093855) and DECRA project (DE140100619), Ministry of Science and Technology (2012DFR40240) and partially supported from the China Scholarship Council (CSC, No. 201306030039). Authors acknowledge use of JEOL 2010 within the UoW Electron Microscopy Centre.

Notes and references

1 S. Chu, A. Majumdar, *Nature* 2012, **488**, 294-303.
2 Y. Liang, Y. Li, H. Wang, J. Zhou, J. Wang, T. Regier, H. Dai, *Nat. Mater.*, 2011, **10**, 780-786.
3 D. Su, H. Jin, Y. Gong, M. Li, Z. Pang and Y. Wang, *J. Mater. Chem. A*, 2015, **3**, 11756-11761.
4 Y.-F. Zhao, Z.-Y. Yang, Y.-X. Zhang, L. Jing, X. Guo, Z. Ke, P. Hu, G. Wang, Y.-M. Yan, K.-N. Sun, *J. Phys. Chem. C*, 2014, **118**, 14238-14245.

5 J. Zhang, B. Sun, X. Xie, Y. Zhao and G. Wang, *Adv. Sci.* 2016, **3**, 1500285.
6 C.C. Pavel, F. Cecconi, C. Emiliani, S. Santiccioli, A. Scaffidi, S. Catanorchi, M. Comotti, *Angew. Chem. Int. Ed.*, 2014, **53**, 1378-1381.
7 M.G. Walter, E.L. Warren, J.R. McKone, S.W. Boettcher, Q. Mi, E.A. Santori, N.S. Lewis, *Chem. Rev.*, 2011, **111**, 5815-5815.
8 Y. Yu, S.-Y. Huang, Y. Li, S.N. Steinmann, W. Yang, L. Cao, *Nano Lett.*, 2014, **14**, 553-558.
9 S. Chen, J. Duan, Y. Tang, B. Jin, S.Z. Qiao, *Nano Energy*, 2015, **11**, 11-18.
10 W.-F. Chen, J.M. Schneider, K. Sasaki, C.-H. Wang, J. Schneider, S. Iyer, S. Iyer, Y. Zhu, J.T. Muckerman, E. Fujita, *Chemsuschem*, 2014, **7**, 2414-2418.
11 S. Wang, J. Wang, M. Zhu, X. Bao, B. Xiao, D. Su, H. Li and Y. Wang, *J. Am. Chem. Soc.*, 2015, **137**, 15753-15759.
12 M. Jahan, Z. Liu, K.P. Loh, *Adv. Funct. Mater.*, 2013, **23**, 5363-5372.
13 Y. Zhao, B. Sun, X. Huang, H. Liu, D. Su, K. Sun, G. Wang, *J. Mater. Chem. A*, 2015, **3**, 5402-5408.
14 Y. Hou, J. Li, Z. Wen, S. Cui, C. Yuan, J. Chen, *Nano Energy*, 2015, **12**, 1-8.
15 X. Liu, Z. Chang, L. Luo, T. Xu, X. Lei, J. Liu, X. Sun, *Chem. Mater.*, 2014, **26**, 1889-1895.
16 L.D. Rafailovic, C. Gammer, C. Rentenberger, T. Trisovic, C. Kleber, H.P. Karnthaler, *Nano Energy*, 2013, **2**, 523-529.
17 G. Wu, K.L. More, C.M. Johnston, P. Zelenay, *Science*, 2011, **332**, 443-447.
18 J. Ren, M. Antonietti, T.-P. Fellinger, *Adv. Energy Mater.*, 2015, **5**, 1401660.
19 D.-W. Wang, D. Su, *Energy Environ. Sci.*, 2014, **7**, 576-591.
20 Y. Hou, Z. Wen, S. Cui, S. Ci, S. Mao, J. Chen, *Adv. Funct. Mater.*, 2015, **25**, 872-882.
21 X. Zou, X. Huang, A. Goswami, R. Silva, B.R. Sathe, E. Mikmekova, T. Asefa, *Angew. Chem. Int. Ed.*, 2014, **53**, 4372-4376.
22 W. Zhou, J. Zhou, Y. Zhou, J. Lu, K. Zhou, L. Yang, Z. Tang, L. Li, S. Chen, *Chem. Mater.*, 2015, **27**, 2026-2032.
23 J. Deng, P. Ren, D. Deng, X. Bao, *Angew. Chem. Int. Ed.*, 2015, **54**, 2100-2104.
24 P.S. Kumar, J. Sundaramurthy, S. Sundarrajan, V.J. Babu, G. Singh, S.I. Allakhverdiev, S. Ramakrishna, *Energy Environ. Sci.*, 2014, **7**, 3192-3222.
25 B. Kumar, M. Asadi, D. Pisasale, S. Sinha-Ray, B.A. Rosen, R. Haasch, J. Abiade, A.L. Yarin, A. Salehi-Khojin, *Nat. Commun.*, 2013, **4**, 2819.
26 Y. Yu, L. Gu, C. Zhu, P.A. van Aken, J. Maier, *J. Am. Chem. Soc.*, 2009, **131**, 15984-15985.
27 Y. Aykut, *ACS Appl. Mater. Interfaces*, 2012, **4**, 3405-3415.
28 S. Cavaliere, S. Subianto, I. Savych, D.J. Jones, J. Roziere, *Energy Environ. Sci.,* 2011, **4**, 4761-4785.
29 H. Zhu, M. Du, M. Zhang, M. Zou, T. Yang, S. Wang, J. Yao, B. Guo, *Chem. Commun.*, 2014, **50**, 15435-15438.
30 I. Jeong, J. Lee, K.L.V. Joseph, H.I. Lee, J.K. Kim, S. Yoon, J. Lee, *Nano Energy*, 2014, **9**, 392-400.
31 Y. Ito, W. Cong, T. Fujita, Z. Tang, M. Chen, *Angew. Chem. Int. Ed.*, 2015, **54**, 2131-2136.
32 D. Deng, L. Yu, X. Chen, G. Wang, L. Jin, X. Pan, J. Deng, G. Sun, X. Bao, *Angew. Chem. Int. Ed.*, 2013, **52**, 371-375.
33 J. Suntivich, K.J. May, H.A. Gasteiger, J.B. Goodenough, Y. Shao-Horn, *Science*, 2011, **334**, 1383-1385.
34 T.Y. Ma, J.L. Cao, M. Jaroniec, S.Z. Qiao, *Angew. Chem. Int. Ed.*, 2016, **55**, 1138-1142.
35 M. Tavakkoli, T. Kallio, O. Reynaud, A. G. Nasibulin, J. Sainio, H. Jiang, E. I. Kauppinen and K. Laasonen, *J. Mater. Chem. A*, 2016, **4**, 5216-5222.
36 X. Zheng, J. Xu, K. Yan, H. Wang, Z. Wang, S. Yang, *Chem. Mater.*,2014, **26**, 2344-2353.
37 Y. Zheng, Y. Jiao, Y. Zhu, L.H. Li, Y. Han, Y. Chen, A. Du, M. Jaroniec, S.Z. Qiao, *Nat. Commun.*, 2014, **5**, 3783.
38 H. Liang, F. Meng, M. Caban-Acevedo, L. Li, A. Forticaux, L. Xiu, Z. Wang, S. Jin, *Nano Lett.*, 2015, **15**, 1421-1427.
39 J. Nai, H. Yin, T. You, L. Zheng, J. Zhang, P. Wang, Z. Jin, Y. Tian, J. Liu, Z. Tang, L. Guo, *Adv. Energy Mater.*, 2015, **5**, 1401880.
40 X. Lin, X. Li, F. Li, Y. Fang, M. Tian, X. An, Y. Fu, J. Jin and J. Ma, *J. Mater. Chem. A*, 2016, **4**, 6505-6512.
41 H. Wang, Z. Lu, D. Kong, J. Sun, T.M. Hymel, Y. Cui, *ACS Nano*, 2014, **8**, 4940-4947.
42 C.C.L. McCrory, S. Jung, J.C. Peters, T.F. Jaramillo, *J. Am. Chem. Soc.*, 2013, **135**, 16977-16987.
43 B.Y. Xia, Y. Yan, N. Li, H.B. Wu, X.W.D. Lou, X. Wang, *Nat. Energy*, 2016, **1**, 15006.
44 X. Cui, P. Ren, D. Deng, J. Deng, X. Bao, *Energy Environ. Sci.*, 2016, **9**, 123-129.
45 X. Pan, X. Bao, *Accounts. Chem. Res.*, 2011, **44**, 553-562.
46 H. Fei, Y. Yang, Z. Peng, G. Ruan, Q. Zhong, L. Li, E.L.G. Samuel, J.M. Tour, *ACS Appl. Mater. Interfaces*, 2015, **7**, 8083-8087.
47 Y. Zhao, R. Nakamura, K. Kamiya, S. Nakanishi, K. Hashimoto, *Nat. Commun.*, 2013, **4**, 2390.
48 H. Jin, J. Wang, D. Su, Z. Wei, Z. Pang, Y. Wang, *J. Am. Chem. Soc.*, 2015, **137**, 2688-2694.
49 S. Dou, L. Tao, J. Huo, S. Wang, L. Dai, *Energy Environ. Sci,*, 2016, **9**, 1320-1326.

Graphic Abstract